Directed assembly of cell-laden microgels for fabrication of 3D tissue constructs

Yanan Du*, Edward Lo*, Shamsher Ali, and Ali Khademhosseini†

Department of Medicine, Center for Biomedical Engineering, Brigham and Women's Hospital, Harvard Medical School, Cambridge, MA, 02139; and Harvard–MIT Health Sciences and Technology, Massachusetts Institute of Technology, Cambridge, MA 02139

Edited by Robert Langer, Massachusetts Institute of Technology, Cambridge, MA, and approved April 29, 2008 (received for review February 25, 2008)

We present a bottom-up approach to direct the assembly of cell-laden microgels to generate tissue constructs with tunable microarchitecture and complexity. This assembly process is driven by the tendency of multiphase liquid–liquid systems to minimize the surface area and the resulting surface free energy between the phases. We demonstrate that shape-controlled microgels spontaneously assemble within multiphase reactor systems into predetermined geometric configurations. Furthermore, we characterize the parameters that influence the assembly process, such as external energy input, surface tension, and microgel dimensions. Finally, we show that multicomponent cell-laden constructs could be generated by assembling microgel building blocks and performing a secondary cross-linking reaction. This bottom-up approach for the directed assembly of cell-laden microgels provides a powerful and highly scalable approach to form biomimetic 3D tissue constructs and opens a paradigm for directing the assembly of mesoscale materials.

bottom-up | hydrogel | microscale engineering | biomimetic

Most living tissues are composed of repeating units on the scale of hundreds of microns, which are ensembles of different cell types with well defined 3D microarchitectures and tissue-specific, functional properties (i.e., islet, nephron, or sinusoid) (1). To generate engineered tissues, the recreation of these structural features is of great importance in enabling the resulting function. However, most tissue engineering approaches rely on self-assembly of cells to recreate these complex structures on biodegradable scaffolds, which often does not occur properly (2). Thus, one of the major challenges in tissue engineering is to engineer biomimetic tissues that contain appropriate cell-microenvironmental interactions (cell–cell, cell–matrix, and cell-soluble factors) as well as multicellular architectural features, such as repeating tissue units and proper vascular structure (3, 4). The merger of microscale technologies with hydrogels has generated opportunities for addressing this challenge through the fabrication of biologically relevant microengineered hydrogels with sizes ranging from <1 μm (subcellular level) to >1 cm (tissue level) (5, 6).

Microgels are attractive for tissue engineering applications because of their physical properties (i.e., well defined shapes, mechanical strength, and biodegradability) and biological parameters [i.e., biocompatibility, resemblance to the natural extracellular matrix (ECM), and ability to entrap cells at tissue densities] (7–10). Currently, two different approaches, namely "top-down" or "bottom-up," have emerged in the use of microgels for tissue engineering (5, 6). Top-down approaches control the microscale features (i.e., shape and size) of relatively large pieces of hydrogels (11–13). Alternatively, bottom-up approaches aim to generate larger tissue constructs by the assembly of smaller building blocks (usually cell-laden microgels), which mimics the *in vivo* tissue structure of repeating functional units (5).

To date, bottom-up assembly of microgels has been achieved by random packing of cell-laden microgels (14), by using photolithography to build layers of microgels with controlled alignment (15), or by physical manipulation of individual cell-laden microgels (16). However, a number of potential limitations exist with these approaches. For example, a random packing process cannot be used to control the resulting hydrogel structure and orientation, which may be essential in recreating biomimetic tissue complexity. Also, manual manipulation and photolithography are difficult to scale-up, slow, and involve multiple steps. To generate microengineered tissue constructs by using bottom-up approaches, a "self-assembly" process that enables assembly of microscale tissue units in a directed and scalable manner is desirable.

Whitesides and coworkers (17–19) pioneered a mesoscale self-assembly approach to build millimeter-scale objects into well defined 2D or 3D structures through minimization of the interfacial free energy of the liquid–liquid interface. However, this bottom-up approach cannot be used to build tissue constructs because of the cytotoxicity of the materials and the harsh operations involved in the process (i.e., high temperature, toxic reagents). In this article, we present the first attempt to assemble cell-laden microgel units into tissue constructs with tunable 3D structures in a highly scalable manner. In this approach, we used the thermodynamic tendency of multiphase liquid–liquid systems to minimize their contact surfaces (i.e., the tendency of oil and water to segregate). In the presence of water and a hydrophobic phase, this tendency is called the "hydrophobic effect" in which the interaction free energy, which is proportional to the solvent-exposed surface area, tends to minimize (20). We hypothesized that the hydrophobic effect, which is used as the driving force for a number of other applications (17, 20, 21), could be used to assemble microgels in a directed manner. Thus, we envisioned that by agitating hydrophilic microgels in hydrophobic medium, the microgel units would assemble in an organized manner to locally minimize the interaction free energy (the surface area exposed to the oil).

Results and Discussion

To test the hydrophobic effect, poly(ethylene glycol) (PEG) microgels were synthesized by using photolithography (total number, 500), transferred into hydrophobic mineral oil phase, and assembled upon application of a controlled agitation force (Fig. 1). Upon examination, four types of microgel assembly were observed: linear, branched, random, and offset (offset was only observed in the presence of surfactant as discussed later). Because the hydrophobic effect minimizes the oil–water inter-

Author contributions: Y.D., E.L., S.A., and A.K. designed research; Y.D., E.L., and S.A. performed research; Y.D., E.L., S.A., and A.K. analyzed data; and Y.D., E.L., and A.K. wrote the paper.

The authors declare no conflict of interest.

This article is a PNAS Direct Submission.

Freely available online through the PNAS open access option.

*Y.D. and E.L. contributed equally to this work.

†To whom correspondence should be addressed at: 65 Landsdowne Street, Cambridge, MA 02139. E-mail: alik@mit.edu

This article contains supporting information online at www.pnas.org/cgi/content/full/0801866105/DCSupplemental.

© 2008 by The National Academy of Sciences of the USA

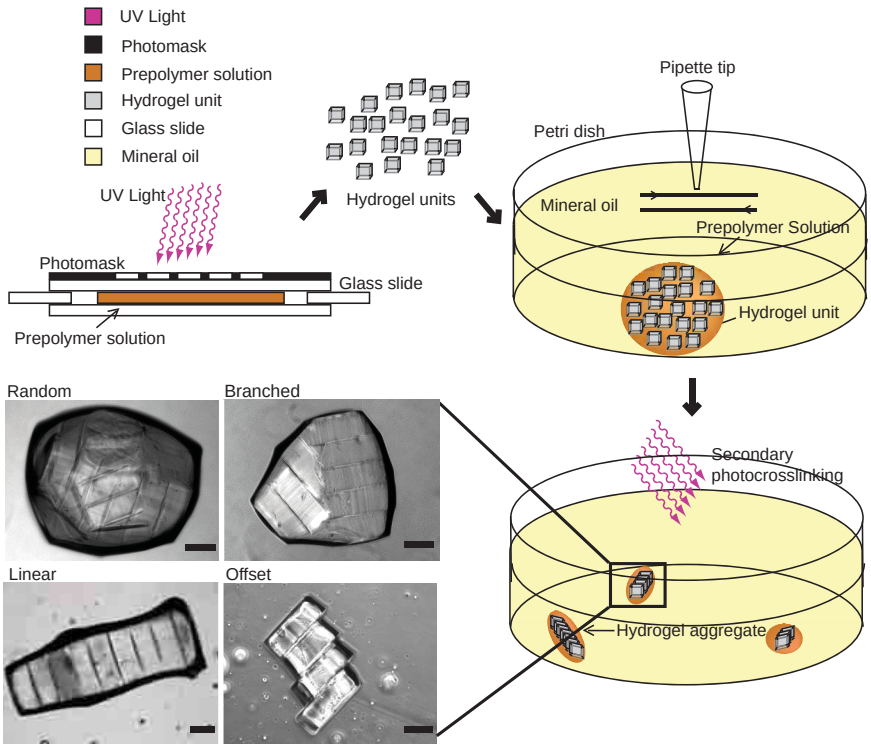

Fig. 1. Schematic diagram of microgel assembly process. Microgel units were synthesized by photolithography, transferred into a dish containing mineral oil, and subjected to mechanical agitation applied by manually manipulating a pipette-tip in a back-and-forth manner. Four structural types of microgel assemblies were observed: linear, branched, random, and offset. Secondary cross-linking was achieved by exposing the microgel assemblies to UV light. (Scale bars, 200 μm.)

face, which for water will be spherical droplets, the optimum geometry for the case in which rectangular hydrogels are assembled will be 1:1 aspect ratio cubes composed of packed rectangular hydrogels. In our case, we were interested in the fraction of assemblies that gave rise to linear segments, because for small chain lengths, they led to the most thermodynamically favorable outcome.

To analyze the rate of formation of different types of assemblies, the effects of agitation rate and time, and the addition of surfactant were investigated by using rectangular microgels (Fig. 2). To change the amount of energy used to stir the mixture, we changed the agitation rate. It was found that faster agitation, as indicated by higher Reynolds numbers, generated a larger fraction of linear assemblies (up to 30% at 15 s) (Fig. 2*A*). It is important to note that the upper range of tested Reynolds numbers was limited to a value of 3 (indicating laminar flow) given the viscous nature of the mixing solution and the experimental setup. To assess the effects of agitation time, we kept the agitation at Re = 3, and we analyzed the assembly formation over time. We observed that longer agitation time resulted in an asymptotic increase in the fraction of linear microgel assemblies within the first 60 s. Beyond this agitation time, the percentages of linear microgel assemblies remained constant (Fig. 2*B*). Therefore, higher agitation rate and longer agitation time are thought to input more energy and generate more linear and branched hydrogel assemblies, which could keep the two-phase system in a lower energy state compared with random hydrogel assemblies. In addition, we analyzed the chain lengths of the resulting hydrogel assemblies to validate our hypotheses regarding preferred assembly aspect ratios. We observed that, in most cases, the average chain length of the linear microgel assemblies was ≈3 units. This length was expected given the microgel dimensions of 400 (length) × 400 (width) × 150 (height) μm and that stacks of three vertically aligned microgels represented an aspect ratio of approximately 1. Furthermore, we observed the formation of low-frequency assemblies with high chain lengths that we anticipate will be the result of mergers of several smaller aggregates [see supporting information (SI) *Text* and Figs. S1–S3].

Surface tension is the driving force for the induction of microgel assembly in the attempt to minimize their exposure to the oil phase. To study the effects of changes in the driving force of the assembly process, we altered the surface tension of the oil/water interface by using a surfactant. In these experiments, Tween 20 was added to the mineral-oil phase to reduce the surface tension. As expected, the addition of surfactant dramatically decreased the directed-assembly driving force (Fig. 2*C*), because both the percentages of linear and branched assemblies decreased with increasing surfactant concentrations, whereas the fraction of random assemblies increased. Also, in the presence of reduced surface tension, "offset" assemblies were observed in which individual hydrogels were loosely stacked. These assemblies presented an interesting balance between the competing hydrophobic effects that induced aggregation and the hydrodynamic effects in the viscous oil phase.

We also analyzed the effects of changing the dimension of individual microgel units on the formation of microgel assemblies. In these studies, we kept the height constant at 150 μm and increased the length and width of the microgels from 200 to 1,000 μm in 200-μm increments. After inducing assembly formation, we observed that smaller microgels (aspect ratios of 1.3, 2.6, and 4) formed higher fractions of linear and branched assemblies and lower fractions of random assemblies than larger microgels (aspect ratios of 5.3 and 6.6) (Fig. 3*A*). This may be the result of increased hydrodynamic and drag forces that are experienced by larger microgels that overcome the forces associated with the hydrophobic effect. In addition, we analyzed the average chain length of the linear fractions of the microgel assemblies made

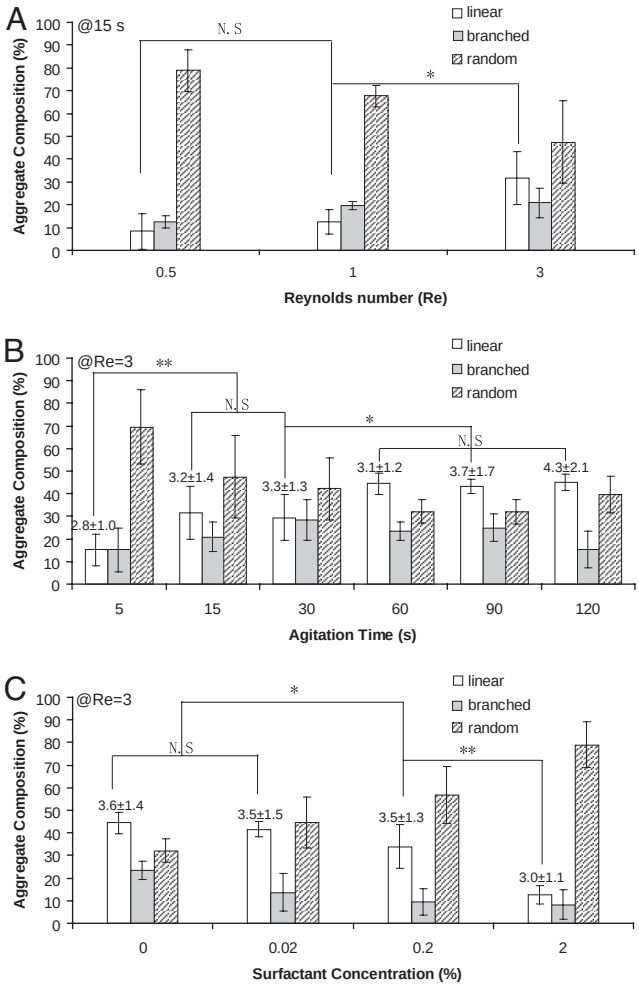

Fig. 2. Optimization of the microgel assembly. Effects of (*A*) agitation rate (fast, medium, and slow), (*B*) agitation time, and (*C*) the addition of surfactant on microgel assembly. Compositions of linear, branched, or random microgel assemblies were compared. Average chain length of linear assemblies with SD was also labeled in *B* and *C*. Data are means ± SD, $n = 3$. *, $P < 0.05$; **, $P < 0.01$. N.S., not significant.

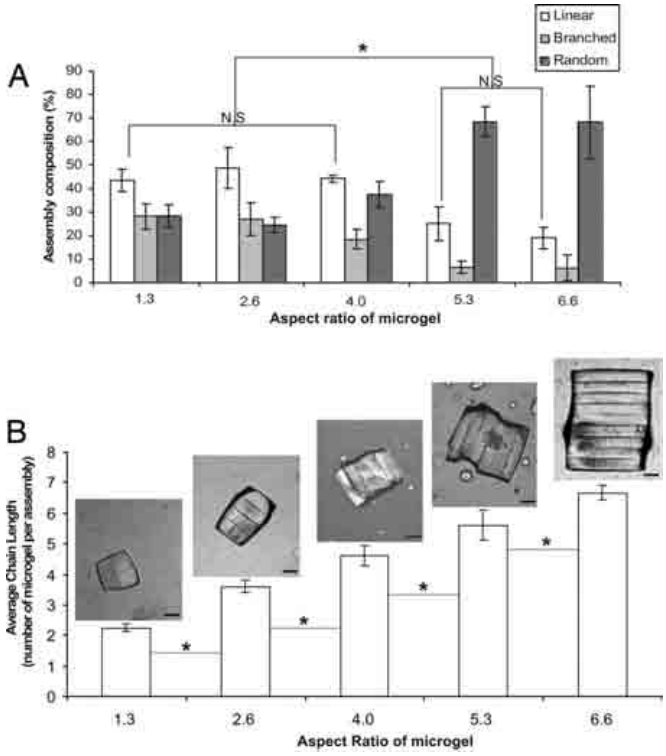

Fig. 3. Effects of the microgel dimensions on microgel assembly. (*A*) Assembly composition and (*B*) average chain length of linear, branched, or random microgel assemblies containing microgel units with different aspect ratios were compared (phase image in *B*). Data are means ± SD, $n = 3$. *, $P < 0.05$. N.S., not significant.

with microgels of different sizes. We observed that as predicted, the average chain length of microgel assemblies corresponded to the aspect ratios of the microgels, such that the resulting microgel assemblies had an approximate aspect ratio of 1 (Fig. 3*B*). Also, nearly cubic microgels with an aspect ratio of 1.3 formed a large fraction of square structures that minimized microgel exposure to the oil phase (Fig. 3*B*). Our results confirm our hypothesis that larger aspect ratio microgels result in the formation of chains with more units in the attempt to minimize microgel contact with the oil phase.

Although the two-phase assembly process can be used to direct the assembly of microgels, these structures were unstable outside of the oil phase (Fig. 4*A*). To stabilize the interaction between assembled microgel structures, we used a secondary cross-linking step (Fig. 1). Secondary cross-linking with a UV exposure time of 4 s was sufficient to stabilize the microgel assemblies (Fig. 4*B*). Residual prepolymer solution surrounding individual microgels before agitation was necessary for the success of the secondary cross-linking. When microgel units were washed with PBS to remove residual prepolymer solution, microgel assemblies that formed after agitation dissociated in culture medium even after secondary UV exposure (Fig. 4*C*). We also demonstrated that there was a slight amount of residual mineral oil on the surface of the hydrogels (see results in *SI Text* and Figs. S1–S3). However, because mineral oil has been used as an inert and safe reagent in many biomedical investigations (22, 23), we do not expect that the residual oil on the surface of the hydrogel assemblies will have cytotoxic effects. Furthermore, we believe that by modifying our process and by using more hydrophilic hydrogels, we can minimize the amount of residual oil that remains on the surface of the gels.

The assembly of microgels with defined 3D structures is a potentially promising approach for bottom-up engineering of tissue constructs, which mimic the complexity of living tissues. Because the exchange of soluble factors among different hydrogel components are vital for cell survival and signaling (24), mass transfer between the microgels was investigated by assembling a mixture of microgels labeled with rhodamine-dextran [molecular mass (M_r) = 10 kDa] or FITC-dextran (M_r = 2,000 kDa). We observed that within the time required to form the assemblies (1 min), rhodamine-dextran was able to freely diffuse in and out of the hydrogel (Fig. 4*D*), whereas FITC-dextran was shown to diffuse very slowly through the microgels because of its larger size (see results in *SI Text* and Figs. S1–S3). Upon assembly of the stained microgels, rhodamine-dextran diffused throughout the hydrogel construct, indicating the barrier-free diffusion between the microgels (Fig. 4*E*). As a negative control, we showed that Nile red, a hydrophobic dye that adsorbed to the hydrophobic domains of PEG hydrogel, did not diffuse throughout the hydrogel, resulting in microgels that were distinctively stained with red or green dye in the final hydrogel assemblies (Fig. 4*F*). To validate the ability of assembling microgels containing different cell types to mix based on their ratios, fluorescent microbeads were used to label different ratios of microgels (Fig. 4 *G–I*). Microbead-containing and plain microgels were

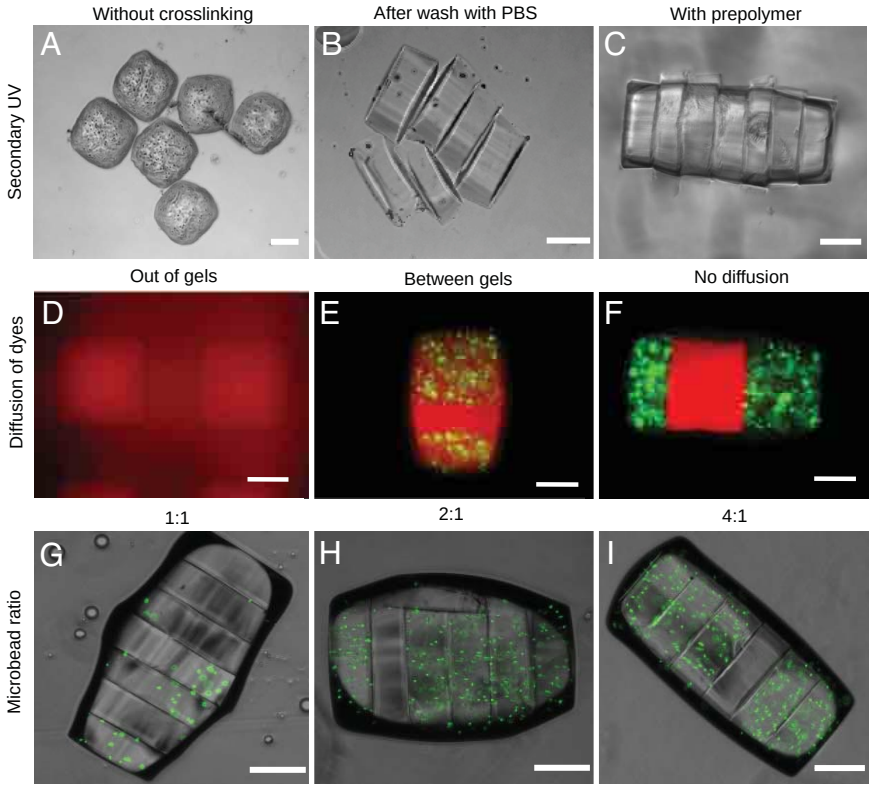

Fig. 4. Secondary cross-linking of the microgel assembles. (*A*) Dissociated microgel assemblies after replacing mineral oil with culture medium without secondary cross-linking. (*B*) Stabilized microgel assemblies in culture medium after secondary cross-linking. (*C*) Dissociated microgel assemblies after secondary cross-linking with removed residual prepolymer. (*D–F*) Diffusion of dyes through the hydrogel. (*D*) Free diffusion of rhodamine-dextran (M_r = 10 kDa) out of the hydrogel into PBS. (*E*) Two groups of microgels labeled with rhodamine-dextran or FITC-dextran (M_r = 2,000 kDa) were assembled, and the rhodamine-dextran diffused throughout the entire hydrogel assembly. (*F*) Microgel assemblies with FITC-dextran- or Nile red-stained microgels. (*G–I*) Microbead-containing and plain microgels were used to model microgels containing two types of cells by varying the initial mixing ratios of these two types of microgels (1:1, 2:1, and 4:1, respectively). (Scale bars, 200 μm.)

mixed in different ratios and subjected to agitation. We observed that the final ratio of the two types of microgels in the hydrogel assemblies often were proportional to the initial mixing ratios.

To validate the use of the microscale hydrogel assembly process developed here for biological applications, we encapsulated cells within PEG microgels and confirmed the viability of cells by using calcein AM-ethidium homodimer. Within these hydrogels, a high fraction of cells remained viable immediately after cell encapsulation. Furthermore, we observed that the assembly process can be used to induce directed assembly of cell-laden microgels while maintaining high cell viability (Fig. 5*A*). To further characterize this process, we analyzed the effects of each step on the microgel assembly process (agitation rate: Re = 3, agitation time: 1 min) (Fig. 5*B*). We observed that the prepolymer solution and the initial cross-linking step did not result in a significant amount of cell death to the encapsulated NIH 3T3 fibroblasts, similar to previously published studies (16, 25). Surprisingly, a slight loss of cell viability was observed during the agitation step while the hydrogels were immersed in the hydrophobic phase. This may be due to water-soluble contaminants derived from the hydrophobic phase. As expected, the duration of UV exposure during each cross-linking step greatly influenced cell viability, and we independently confirmed that the reduction in UV exposure time can significantly reduce the cytotoxic effects of photo cross-linking on cell viability.

So far, although the overall dimensions and architecture of the final hydrogel assembly could be controlled, the assembly of individual microgels was random. For example, the direct alignment of one type of gel next to another was not controllable. To demonstrate the utility of this approach for generating more complex and "directed" structures, we used a "lock-and-key" design for the microgel shapes to control the relative position of two types of microgels in the final assembly. As shown in Fig. 6, microgels with cross and rod shapes (Fig. 6 *A* and *B*) could be assembled in a directed manner with one cross-shaped microgel assembling with one, two, or three rod-shaped microgels (Fig. 6 *C–H*). We achieved ≈10% lock-and-key assemblies by using our current assembly approach without any optimization steps. In addition, we demonstrated the application of the lock-and-key directed assembly for generating cellular cocultures. In this process, we encapsulated cells stained with red or green cell tracker into cross-shaped or rod-shaped microgels and fabricated microscale tissue constructs composed of two types of cells (Fig. 6 *I* and *J*).

In conclusion, we introduced an approach that utilizes the thermodynamic properties of multiphase liquid–liquid systems to assemble microscale cell-laden hydrogels. We demonstrated that hydrogel assembly can be controlled by the forces involved in minimizing the surface free energy between the phases. This bottom-up approach for the directed assembly of cell-laden microgels provides a powerful and highly scalable approach to the formation of 3D tissue constructs by the directed assembly of microengineered units. With the increasing capability of photolithographic approaches to generate microfabricated tissue structures, we envision a potential opportunity to use this technique to create higher-order structures that may be difficult and time consuming to fabricate by using conventional microengineering systems.

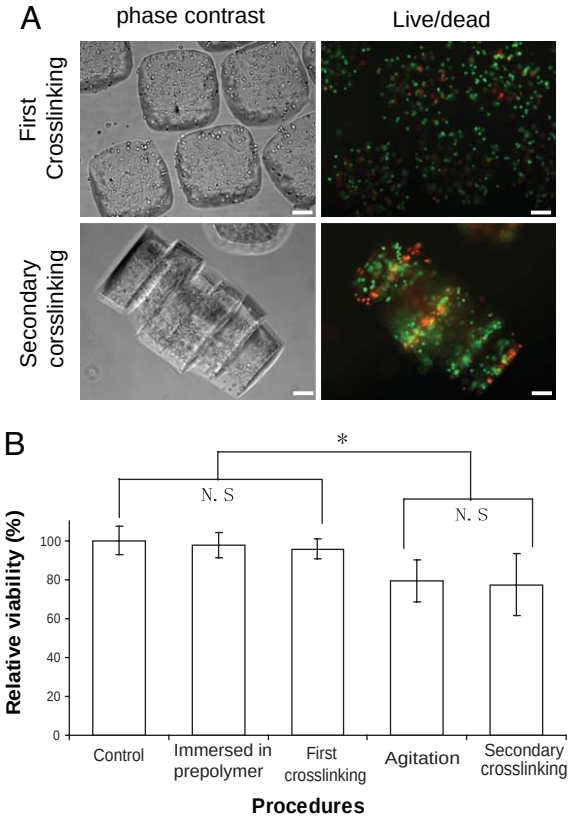

Fig. 5. Cell-laden microgel assemblies. (*A*) Phase-contrast and fluorescence images of cell-laden (NIH 3T3) microgel assemblies after first and secondary cross-linking, respectively, to show the morphology. (*B*) Quantified cell viability after each step in the procedure to form hydrogel aggregates. (Scale bars, 100 μm.)

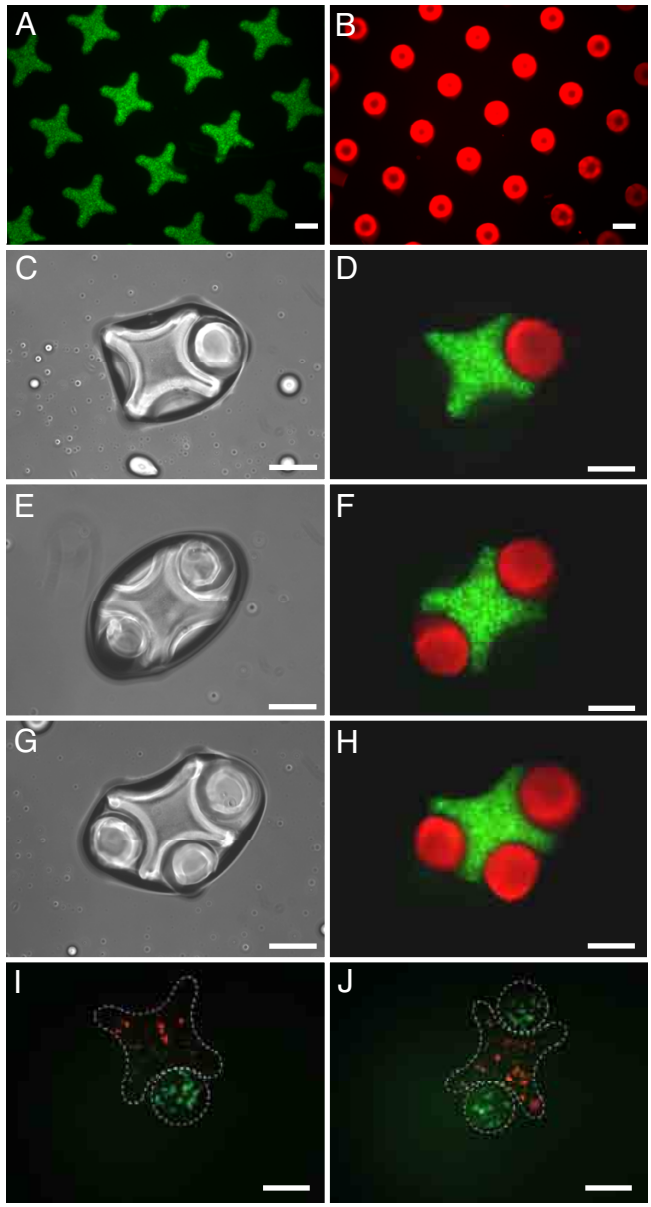

Fig. 6. Directed assembly of lock-and-key-shaped microgels. (*A*) Fluorescence images of cross-shaped microgels stained with FITC-dextran. (*B*) Rod-shaped microgels stained with Nile red. (*C–H*) Phase-contrast and fluorescence images of lock-and-key assemblies with one to three rods per cross. (*I* and *J*) Fluorescence images of microgel assembly composed of cross-shaped microgels containing red-stained cells, and rod-shaped microgels containing green-stained cells. (Scale bars, 200 μm.)

Materials and Methods

Materials. All reagents were purchased from Sigma–Aldrich, unless specifically mentioned otherwise.

Fabrication of Microgel Units by Photolithography. Prepolymer solution was prepared by dissolving 20% (wt/wt) poly(ethylene glycol)-methacrylate polymer, (PEGmA, M_r = 1,000 Da; Sigma) in Dulbecco's Phosphate Buffered Saline (DPBS; GIBCO). Immediately before UV polymerization, 1% photoinitiator (wt/wt), 2-hydroxy-1-(4-(hydroxyethoxy) phenyl)-2-methyl-1-propanone (Irgacure 2959; CIBA Chemicals) was added to the prepolymer solution. Photomasks with square patterns (dimensions: 200 × 200, 400 × 400, 600 × 600, 800 × 800, and 1,000 × 1,000 μm) as well as the lock-and-key shapes were designed by using AutoCAD and printed on transparencies with 20,000-dpi resolution (CAD/Art Services). A drop containing 30 μl of the photo cross-linkable PEGmA prepolymer and photoinitiator was pipetted onto an 18 × 18-mm coverslide between two spacers (one 150 μm thick, 18 × 18-mm coverslide on opposite sides) (Fig. 1). Another 18 × 18-mm coverslide was applied on top of the solution drop, which formed an evenly distributed film of prepolymer solution between the two glass slides with a height of 150 μm. Subsequently, a photomask was placed on the top glass slide, and microgels were formed by exposing the prepolymer solution to UV light (360–480 nm; 12.4 mW/cm^2) through the photomask for 30 s. By using photomasks with different dimensions (200 × 200 × 150, 400 × 400 × 150, 600 × 600 × 150, 800 × 800 × 150, and 1,000 × 1,000 × 150 μm), microgels with different aspect ratios were generated. Aspect ratios were calculated by dividing microgel length by height.

Assembling Microgels at the Oil–Water Interface by Mechanical Agitation. After UV exposure, the top coverslide and spacers were carefully removed. Microgel units (total number = 500) soaked in prepolymer solution were transferred to a 60 × 15-mm dish (Fisher Scientific) containing 6 ml of mineral oil (CVS Pharmacy). Microgel units were assembled at the oil–water interface by mechanical agitation, which was applied by manually manipulating a pipette tip to sketch straight lines. Various agitation rates and times were investigated to optimize the assembly. The agitation rate was expressed by the Reynolds number, which was calculated by $\mathrm{Re} = \rho V_s L/\mu$, where Re is the Reynolds number; μ is the dynamic fluid viscosity ($\approx$1g/cm·s^{-1}); L is the characteristic length of the pipette tip ($\approx$1 mm); V_s is the mean velocity of moving pipette tip (manually achievable velocities range from 6 to 36 cm·s^{-1}); ρ is the density of the oil ($\approx$1g·cm^{-3}). To investigate the effect of the surfactant on microgel assembly, Tween 20 was added to 15-ml tubes containing 6 ml of mineral oil, at volume ratios of 0.02%, 0.2%, and 2%, and mixed by vortexing for 5 min. Microgel units were assembled at the surfactant-containing oil–water interface as described previously.

Secondary Cross-Linking to Stabilize the Microgel Assembly. Microgel assemblies formed in mineral oil were exposed to secondary UV cross-linking for 4 s

to stabilize the structure. To label individual microgels, fluorescein isothiocyanate-dextran (FITC-dextran, M_r 2,000 kDa), rhodamine-dextran (M_r = 10 kDa), Nile red (M_r = 317 Da), or green fluorescent microbeads (1% solid, D = 5 μm; Duke Scientific) were mixed with prepolymer solution at a concentration of 0.2 mM, or 0.02% for microbeads, before photo cross-linking.

Fabrication of Cell-Laden Microgel Assemblies. NIH 3T3 mouse fibroblast cells were maintained in DMEM supplemented with 10% FBS in a 5% CO_2 humidified incubator at 37°C. To encapsulate NIH 3T3 cells within the prepolymer solution, the cells were trypsinized and resuspended in the prepolymer solution at a concentration of 1×10^7cells per ml. Cell-laden microgels and microgel assemblies were generated based on the optimized assembly conditions from the above-mentioned experiments. Cell viability was characterized by incubating cells with Live/Dead dyes (2 μl of Calcein AM and 0.5 μl of Ethidium homodimer-1; Molecular Probes) in 1 ml of DPBS for 10 min. Cells were labeled green with Calcein AM and labeled red with PKH26 Red Fluorescent Cell Linker.

ACKNOWLEDGMENTS. We thank Drs. Utkan Demirci and Edward Haeggstrom and Mr. Masoud Khabiry for the scientific discussions. This work was supported by the National Institutes of Health, the Coulter Foundation, and the Institute for Soldier Nanotechnology. Y.D. was funded by the U.S. Army Construction Engineering Research Laboratory, Engineering Research and Development Center (USACERL/ERDC).

1. Costanzo L (2006) *Physiology*, (Saunders, Philadelphia), 3rd Ed.
2. Langer R, Vacanti JP (1993) Tissue engineering. *Science* 260:920–926.
3. Griffith LG, Swartz MA (2006) Capturing complex 3D tissue physiology *in vitro*. *Nat Rev Mol Cell Biol* 7:211–224.
4. Levenberg S, *et al.* (2005) Engineering vascularized skeletal muscle tissue. *Nat Biotechnol* 23:879–884.
5. Khademhosseini A, Langer R (2007) Microengineered hydrogels for tissue engineering. *Biomaterials* 28:5087–5092.
6. Khademhosseini A, Langer R, Borenstein J, Vacanti JP (2006) Microscale technologies for tissue engineering and biology. *Proc Natl Acad Sci USA* 103:2480–2487.
7. Nguyen KT, West JL (2002) Photopolymerizable hydrogels for tissue engineering applications. *Biomaterials* 23:4307–4314.
8. Ifkovits JL, Burdick JA (2007) Review: Photopolymerizable and degradable biomaterials for tissue engineering applications. *Tissue Eng* 13:2369–2385.
9. Lee KY, Mooney DJ (2001) Hydrogels for tissue engineering. *Chem Rev* 101:1869–1879.
10. Hoffman AS (2001) Hydrogels for biomedical applications. *Ann NY Acad Sci* 944:62–73.
11. Cabodi M, *et al.* (2005) A microfluidic biomaterial. *J Am Chem Soc* 127:13788–13789.
12. Fidkowski C, *et al.* (2005) Endothelialized microvasculature based on a biodegradable elastomer. *Tissue Eng* 11:302–309.
13. Ling Y, *et al.* (2007) A cell-laden microfluidic hydrogel. *Lab Chip* 7:756–762.
14. McGuigan AP, Sefton MV (2006) Vascularized organoid engineered by modular assembly enables blood perfusion. *Proc Natl Acad Sci USA* 103:11461–11466.
15. Liu Tsang V, *et al.* (2007) Fabrication of 3D hepatic tissues by additive photopatterning of cellular hydrogels. *FASEB J* 21:790–801.
16. Yeh J, *et al.* (2006) Micromolding of shape-controlled, harvestable cell-laden hydrogels. *Biomaterials* 27:5391–5398.
17. Bowden N, Terfort A, Carbeck J, Whitesides GM (1997) Self-assembly of mesoscale objects into ordered two-dimensional arrays. *Science* 276:233–235.
18. Breen TL, Tien J, Oliver SR, Hadzic T, Whitesides GM (1999) Design and self-assembly of open, regular, 3D mesostructures. *Science* 284:948–951.
19. Choi IS, Bowden N, Whitesides GM (1999) Macroscopic, hierarchical, two-dimensional self-assembly. *Angew Chem Int Ed Engl* 38:3078–3081.
20. Raschke TM, Tsai J, Levitt M (2001) Quantification of the hydrophobic interaction by simulations of the aggregation of small hydrophobic solutes in water. *Proc Natl Acad Sci USA* 98:5965–5969.
21. Chandler D (2005) Interfaces and the driving force of hydrophobic assembly. *Nature* 437:640–647.
22. Goossens E, Frederickx V, De Block G, Van Steirteghem AC, Tournaye H (2003) Reproductive capacity of sperm obtained after germ cell transplantation in a mouse model. *Hum Reprod* 18:1874–1880.
23. Mirza A, *et al.* (1997) A role for tissue transglutaminase in hepatic injury and fibrogenesis, and its regulation by NF-kappaB. *Am J Physiol* 272:G281–G288.
24. Folch A, Toner M (2000) Microengineering of cellular interactions. *Annu Rev Biomed Eng* 2:227–256.
25. Burdick JA, Chung C, Jia X, Randolph MA, Langer R (2005) Controlled degradation and mechanical behavior of photopolymerized hyaluronic acid networks. *Biomacromolecules* 6:386–391.